Sensing and Bio-Sensing Research 3 (2015) 1–6

Contents lists available at ScienceDirect

Sensing and Bio-Sensing Research

journal homepage: www.elsevier.com/locate/sbsr

Optofluidic spectroscopy integrated on optical fiber platform

Edikan Archibong, Justin Stewart, Anna Pyayt *

Innovative Biomedical Instruments and Systems (IBIS) Lab, Department of Chemical & Biomedical Engineering, University of South Florida, Tampa, FL 33260, United States

ARTICLE INFO

Keywords:
Spectroscopy
Drug monitoring
Optofluidics

ABSTRACT

Administering a wrong drug or a wrong dose can be extremely dangerous and can result in severe adverse effects or even the death of a patient. With human errors being possible, automatic real time identification of a drug and its concentration using technology is a viable option to decrease the chance of incorrect drug administration. As a step toward this goal, we propose a new optical fiber based spectroscopic system that has built-in filtration capabilities and thus can work in real time near patient without additional sample pre-processing. It is designed as a point probe consisting of an optical fiber with a miniature filtering reflector integrated on the interface. In the future it can be inserted into a bag for intravenous therapy (IV therapy) or in a syringe to measure the spectrum of the fluid and to confirm its properties. Additionally, use of microfluidic filtration allows to remove microscopic particles from the sample and thus decreases the noise and increases the sensitivity of spectroscopic measurement. In this study, an optofluidic system was fabricated, and filtration capabilities and measurement of cobalamin (vitamin B_{12}) concentration have been demonstrated.

1. Introduction

The Institute of Medicine estimated that as many as 98,000 patients die each year due to preventable medical errors, making this the sixth leading cause of death in the United States, and claiming more lives than diabetes or Alzheimer disease [1]. Additionally, the expense of medical care necessitated because of medical errors, lost income, and disability, results in a total cost between $17 billion and $29 billion per year [1]. There are many potential sources of error in patient care, such as medical prescriptions, transcriptions, dispensing and administration of drugs, and monitoring patient's responses. However, among these, administration errors account for approximately 32% of morbidity and mortality cases in inpatient facilities [2]. Because of this, there is a pressing need to detect drug identity and concentration during administration, allowing for precise measurement of dosages, and preventing errors in real time before adverse effects take place.

While monitoring of specific medications such as antidepressants and anticoagulants are important for compliance and toxicity checks [3], there are many other pharmaceuticals that when wrongly administered will result in dangerous consequences [2]. Currently, several specialized assay based techniques have been used to monitor medication errors in specific therapeutic treatments, known as therapeutic drug monitoring (TDM) [3–6]. However, assay and label based detection systems such as immunoassays, electrochemical assays, and lateral-flow assays (LFAs) have several limitations that prevent them from being used for point-of-care sensing [7]. These techniques are time consuming, and require large volumes of analyte to achieve the needed sensitivity. Furthermore, drug assays use complicated electrochemical measurements, suffer from background interference in complex solutions and have poor thermal stability [8–14]. Currently there are no available technologies for detection of overdose or incorrect drugs during administration.

There are many sensors that can work in almost real time and do not require use of reagents, but they typically measure refractive index and are based on ring-resonators [23–26], photonic-crystals [15–21], whispering gallery-mode [22–24], plasmonic structures [25] and other optical components, that without additional modifications do not provide enough specificity for differentiation between multiple drugs. In addition, these techniques are prone to noise caused by any microscale particles present in the system and are very sensitive to small temperature changes.

In general, traditional approaches to drug identification include color test [26], microscopic microcrystal analysis [27], thin layer chromatography [28], gas chromatography [29], mass spectroscopy [30], X-ray diffraction [31], and different types of spectroscopy that are most suitable for real time detection. By using traditional spectroscopic techniques (IR, Near-IR, NMR, Raman, etc.) it has been shown that drug identity can be determined [32–35]. Once a drug has been identified using traditional

* Corresponding author. Tel.: +1 813 974 6250.
E-mail address: pyayt@usf.edu (A. Pyayt).

http://dx.doi.org/10.1016/j.sbsr.2014.11.002
2214-1804/

spectroscopy, information regarding concentration may be obtained by quantifying absorption at a specific wavelength. Furthermore, spectroscopy using a single optical fiber is becoming a powerful approach for analysis of biological samples [36–40].

However, for complex systems such as biological fluids that contain a variety of free floating particles and cells, the effectiveness in determining a drugs concentration is significantly reduced due to scattering and interference by these objects. As a result, additional reagents are required to amplify the spectral signatures of compounds of interest (e.g. biomarkers of a specific multiple diseases) [41–43]. Unfortunately, studies requiring reagents and labeling can only be performed in specialized laboratories, using large sample volumes, as well as extensive time for analysis ranging from several hours to multiple days. Because of this, a reliable, reagent and label-free, detection method that can run in real-time by using a small sample volume would greatly benefit point-of care drug monitoring.

To overcome these limitations we have proposed a new optofluidic platform that can be used to detect the concentration of drugs by absorption spectroscopy, free of noise from particles and cells, without prior sample pre-processing. This device is small enough that it can be directly inserted to an IV bag or syringe, and continuously monitor drug concentration before or while the patient is being treated. Additionally, this device can be mass-produced and requires relatively inexpensive materials.

2. Materials and methods

2.1. Device principles

The device was designed to be a compact probe, consisting of a miniature microfluidic chamber attached to the interface of an optical fiber (Fig. 1). The bottom of the microfluidic chamber consists of a porous membrane that allows fluids and chemical compounds to flow inside the device, while at the same time filtering out undesired particles. Furthermore, the porous membrane is coated with a reflective metal. Because of this coating, light will pass through the filtered fluid and reflect back once it reaches the membrane. The reflected light can then be collected by the optical fiber for spectroscopic analysis of the filtered fluid. Based on the absorption of light by the fluid, the system can provide a conclusion if the drug dosage is correct. The top portion of the chamber might also contain small pores to allow air to escape while the chamber is being filled. Alternatively, if the top portion of the chamber is not inserted in fluid, then it might have larger air outlets.

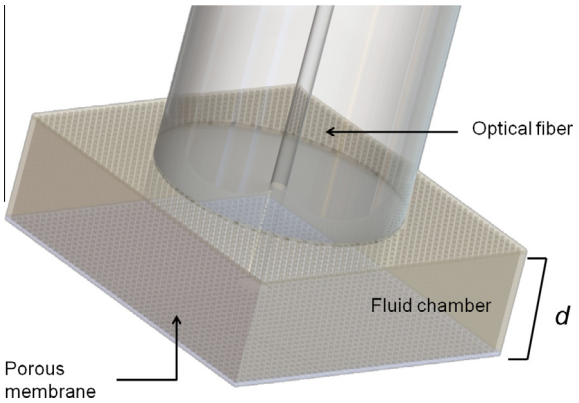

Fig. 1. Artistic rendering of the design of the optofluidic probe and its main components: optical fiber with attached microfluidic chamber. Sample fluid would propagate through the micrometer-size pores while particles are filtered out. The bottom membrane is reflective, so light exiting the fiber into sample fluid contained in the chamber is coupled back into the same fiber for analysis.

2.2. Fabrication flow

The reflective micro-porous membrane for the fluid chamber was fabricated using standard micro-fabrication processes (Fig. 2) [44,45]. Double-side polished silicon wafers purchased from Nova Electronic Materials (Texas) were used as the substrate (Fig. 2a). First, a 1 μm thick membrane layer of silicon nitride (Si_3N_4) was grown on both side of the wafer by low stress–low pressure chemical vapor deposition (LPCVD) at the MiRC facility at Georgia Tech (Fig. 2b). Wafers were cleaned with acetone and IPA, then dried with nitrogen. Additionally, they were bake on hotplate @ 115 °C for 5 min to dehydrate and then cooled for a couple of minutes before spin-coating with photoresist.

Next, Si_3N_4 layer was patterned (Fig. 2c), defining the transparent microfiltering membrane on one side and optic fiber opening on the other side. It was done by spin-coating positive photoresist followed by UV lithography and reactive ion etching on both sides of the wafer. Two consecutive photolithography steps required through-wafer alignment using IR mask aligner. The recipe for the photoresist deposition was the following: 4620AZ Positive Resist was spin-coated first at 4000 rpm for 30 s, then at 500 rpm for 10 s and finally at 6500 rpm for 60 s. This allowed to achieve the most uniform surface coverage. Then it was baked in oven at 100 °C for 20 min and rehydrated for 24 h. The exposure was 7 s on Karl Suss mask aligner (lamp intensity 25 mW/cm^2). After that it was developed for 3 min in photoresist 400 K developer, hard baked at 100 °C for 30 min and used for etching in RIE.

After patterning silicon nitride layers the exposed silicon was etched away in a solution of potassium hydroxide (KOH, 85 °C) for 7 h, creating a hollow chamber between the two nitride layers. This chamber will be filled with the fluid under study through the nitride membrane. Finally, 200 nm of gold was deposited on top of the nitride membrane using a Denton Thermal Evaporator. An optical microscopy image of the micro-fabricated membrane is shown in Fig. 2f. The circular pores of the membrane are 10 μm in diameter, and have been patterned in a square array with the distance of 15 μm from center to center. This configuration of the membrane allows for filtration of particles larger than 10 μm in diameter.

2.3. Filtration experiment

Once the membranes had been prepared, their filtration capabilities were tested. The membranes were pre-wetted and cleaned by flushing them with acetone while switching from sample to

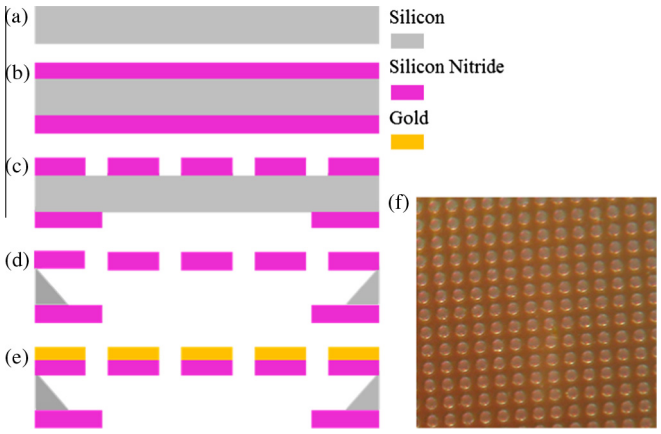

Fig. 2. Device fabrication: (a) two-side polished silicon substrate. (b) Silicon nitride is deposited on both sides of the wafer. (c) Silicon nitride was patterned and etched on both sides. (d) The membrane was released using etching in KOH solution. (e) Gold was deposited on the membrane. (f) Optical microscopy image of a released membrane.

sample. The membranes were positioned underneath an upright optical microscope for observation, where the membrane surfaces were oriented perpendicular to the microscope objective. They were slightly elevated, allowing for space to exist beneath them. In order to observe filtration with these membranes, a droplet of DI water containing naturally occurring contaminants (dust) was placed on top of the membrane surface. By relying on gravitational forces alone, the droplet of water was allowed to pass through the membrane, while contaminants were effectively filtered out. These effects were recorded using a microscope camera. After the filtration experiment was completed, the membranes were easily cleaned by rinsing with acetone.

2.4. Optical experiments

2.4.1. Device packaging

After testing filtering properties of the micro-filtering membranes they were assembled next to the optical fiber tips. For this, an 8 μm optical fiber was cleaved and inserted into an adjustable fiber holder (Fig. 3a) to provide mechanical support to the otherwise flexible fiber. The enlarged image of the exposed fiber tip is shown in Fig. 3b. Following this, the fiber holder was inserted into a high precision XYZ-stage, and the tip was positioned ~105 μm from a reflective metal membrane by adjusting the dial of the optical stage (Fig. 3c). For optical alignment procedures, please refer to the following Section (2.4.2). In Fig. 3d, an enlarged image of the fiber tip and membrane in the assembly is shown. It may be seen that spacing (~105 μm) exists between the fiber and the membrane, and that the membrane itself is coated with gold. Finally, the entire device was fixed in place by epoxying the metal surrounding the membranes to a small polydimethylsiloxane (PDMS) tube. This tube was created to fit tightly to the optical fiber holder, and the final assembly can be seen in Fig. 3e.

2.4.2. Fiber alignment and positioning

As previously stated, before the setup was fixed in place the optical fiber and membrane required alignment and positioning at an appropriate spacing. In order to optimize coupling, the optical fiber was set perpendicular to the membrane. Angular alignment of the system was performed by adjusting the XYZ-stage, and observing the reflected power in air. An approximation of fiber angle was made qualitatively through visual observation. However, for added precision, reflected power was recorded while the fiber angle was finely tuned. The fiber angle was set once the reflected power reach a maximum value.

Following angular alignment, the fiber needed to be placed at a set spacing from the membrane surface. The XYZ-stage allows for vertical adjustment of the fiber. However, micron level precision was needed to effectively determine the spacing, and thus Fabry–Perot resonance was used for high precision measurements. The resonance was formed between the two reflective surfaces – the gold coated membrane and the cleaved fiber interface. The spectrum was recorded in air (refractive index: 1.0) and conducted using infrared light between 1400 and 1500 nm (shown in Fig. 4 for the desired spacing). Using the collected IR spectrum, the distance could be calculated using the following expression:

$$d = \frac{{\lambda_i}^2}{2n(\lambda_{i+1} - \lambda_i)} \quad (1)$$

where λ_i and λ_{i+1} are consecutive resonance wavelengths (nm), n is the refractive index. By recording resonance patterns for different vertical settings of the XYZ-stage, a correlation between stage setting and the actual distance, determined by Eq. (1), was obtained. Once the appropriate vertical setting was found, the fiber was fixed in position and the distance was verified again using Fabry–Perot resonance. In Fig. 4, we can see the Fabry–Perot resonance recorded for the vertical setting once the fiber was set 105 μm from the membrane.

2.4.3. Absorption spectroscopy of Cobalamin

In order to demonstrate that the device is capable of determining drug and its concentrations, absorption spectroscopy was conducted for a specific pharmaceutical – cobalamin (vitamin B_{12}). Different drugs can be identified using UV–vis spectroscopy. For example, absorption spectrum of cobalamin dissolved in water with concentration 60 mg/dL is shown in Fig. 5a. When drug is known, its concentration can be measured at one specific wavelength, since it is much faster than measurements of the whole spectrum.

The goal was to construct a sensor that would be able to conduct measurements for the broad range of concentrations from

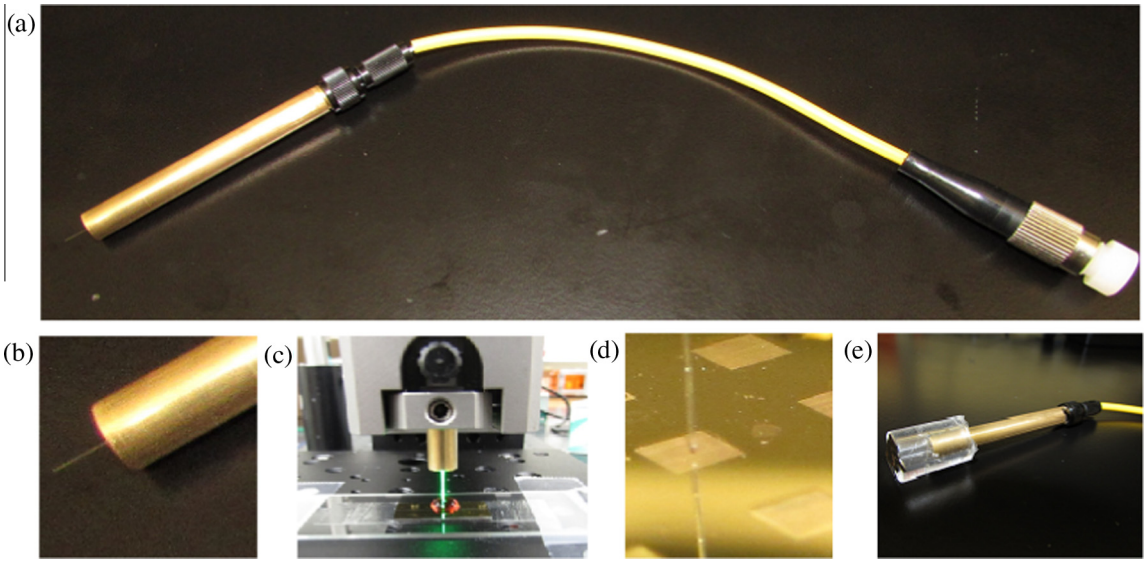

Fig. 3. Details of the packaging. (a) Cleaved optical fiber inserted into fiber holder, (b) enlarged tip of the fiber that is 125 μm in diameter. (c) Optical fiber holder fixed in high precision XYZ-stage. (d) Optical fiber above reflective gold coated membrane. (e) Fully assembled device with an optical fiber enclosed inside of the fluid chamber and a filtering membrane connected at the bottom.

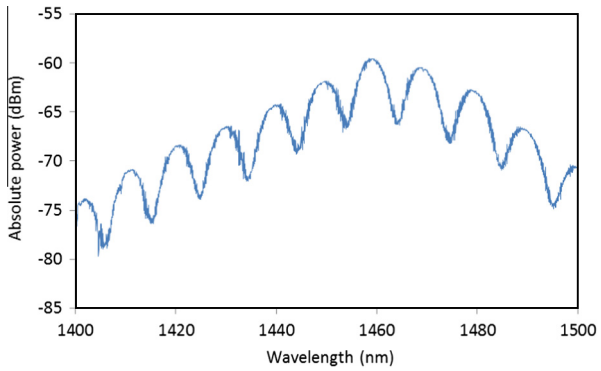

Fig. 4. Fabry–Perot resonance of the set-up used in this experiment. Here the resonance corresponds to a separation of approximately 105 μm between the fiber and reflector.

0.1 mg/dL to 500 mg/dL. Theoretical modeling of this sensors transfer function was conducted using Beer–Lambert law:

$$\frac{P}{P_o} = \exp(-2\alpha d C) \tag{2}$$

where P is the power of transmitted light (W) for the fluid under study, P_o is the transmitted power (W) for a pure sample, α is the molar absorptivity with units of L/mol cm, 2 d is the total optical path where d was the spacing between the fiber and reflective surface (cm), and C is the concentration of the cobalamin expressed in mol/L.

Fig. 5 shows the theoretical transfer functions plotted for the needed range of concentrations and three different spacing between the fiber and the membrane – 75, 105 and 150 μm. While 150 μm gap is better for the measurements of lower concentrations, and 75 μm works better for higher concentrations, the 105 μm gap is suitable for both ranges and thus was chosen for the experimental testing.

During the experiment, the concentration of cobalamin was varied from approximately 0.1–515 mg/dL, while reflected power was recorded for each concentration. All measurements were conducted over 5 min timeframes, during which the power was averaged. A high stability green laser (532 nm) was used at a fixed power at 30 mW. After one cobalamin measurement was made, the sample was removed, and the sensor was thoroughly rinsed with water. This cleaning was conducted to prevent build-up of cobalamin on surfaces. After cleaning, the setup was allowed to air dry for approximately 1 min, ensuring that all water was removed from the system. Samples were tested sequentially with increasing concentration. In order to insure reproducibility of results, every test was calibrated with respect to the water control measurements.

3. Results and discussion

3.1. Filtration demonstration

As previously mentioned, the filtering properties of the microfabricated porous membrane were demonstrated with a drop of DI water. Fig. 6a and b show the empty membrane placed horizontally under the microscope and a membrane right after putting a drop of water, respectively. It may be noticed that the water passes through the pores in the membrane, and forms a drop on the other side, while all particles are filtered by the pores and remain on the membrane surface (Fig. 6b–f). Fig. 6f demonstrates the outline of the water drop that is not fully seen since it is already under the membrane, and the dark spots are particles that are present in all real world samples and were successfully filtered out by the membrane.

For cleaning purposes the membrane was flushed with acetone. It was observed that this also improved its wetting properties. While without applying additional pressure, water goes takes several minutes to completely pass through the membrane. However, prior prewashing decreases this time to seconds (Fig. 6g–i). The membrane was also tested continuously with the lowest setting of a peristaltic pump pumping fluid with the flow rate ~2 μL/s, and it could withstand the external pressure still demonstrating successful particle filtration.

3.2. Optical measurement of cobalamin concentrations

While the proposed optofluidic platform is compatible with a broad range of drugs, here we demonstrated measurements of cobalamin concentration as an example drug that can be monitored using this approach. Cobalamin (vitamin B_{12}) is an essential water-soluble vitamin, of which a deficiency can lead to abnormal neurologic and psychiatric symptoms. This may include ataxia (shaky movements and unsteady gait), muscle weakness, spasticity, incontinence, hypotension (low blood pressure), vision problems, dementia, psychoses, and mood disturbances. There is a variety of doses that are used for injections: from 0.2 μg/kg for neonates and infants to 1000 μg total for adults with severe vitamin deficiency [46]. This means range of concentrations from 1 μg/ml to 1000 μg/ml, therefore the Fig. 7b shows measurements of concentrations between 1 μg /mL to 5 mg/mL to monitor the physiological range and potential overdose.

Because cobalamin was the only compound sensed, all the measurements were conducted with a single wavelength, 532 nm, where cobalamin has high absorption and the sensor would have the highest sensitivity. In future sensing at multiple wavelengths can be used to monitor mixture of several drugs simultaneously.

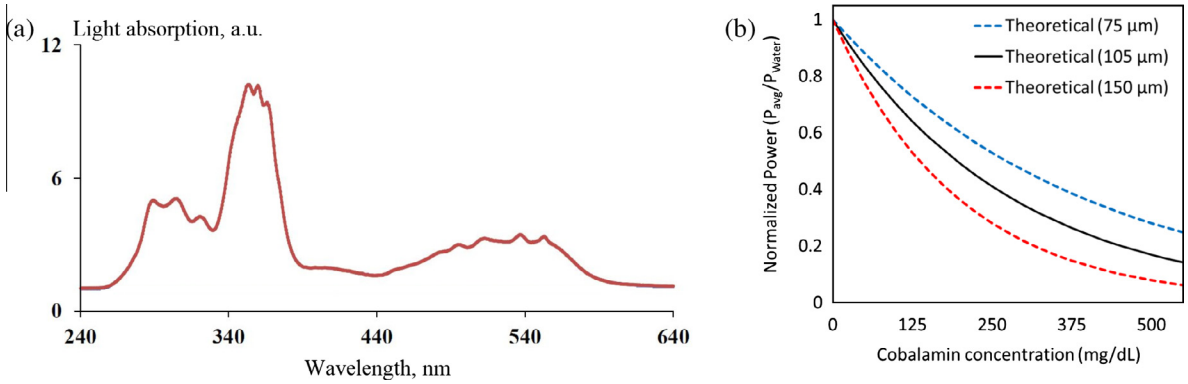

Fig. 5. Experimental absorption spectrum (a) and theoretical transmission profiles for Cobalamin (b) at varying concentrations and fiber spacing.

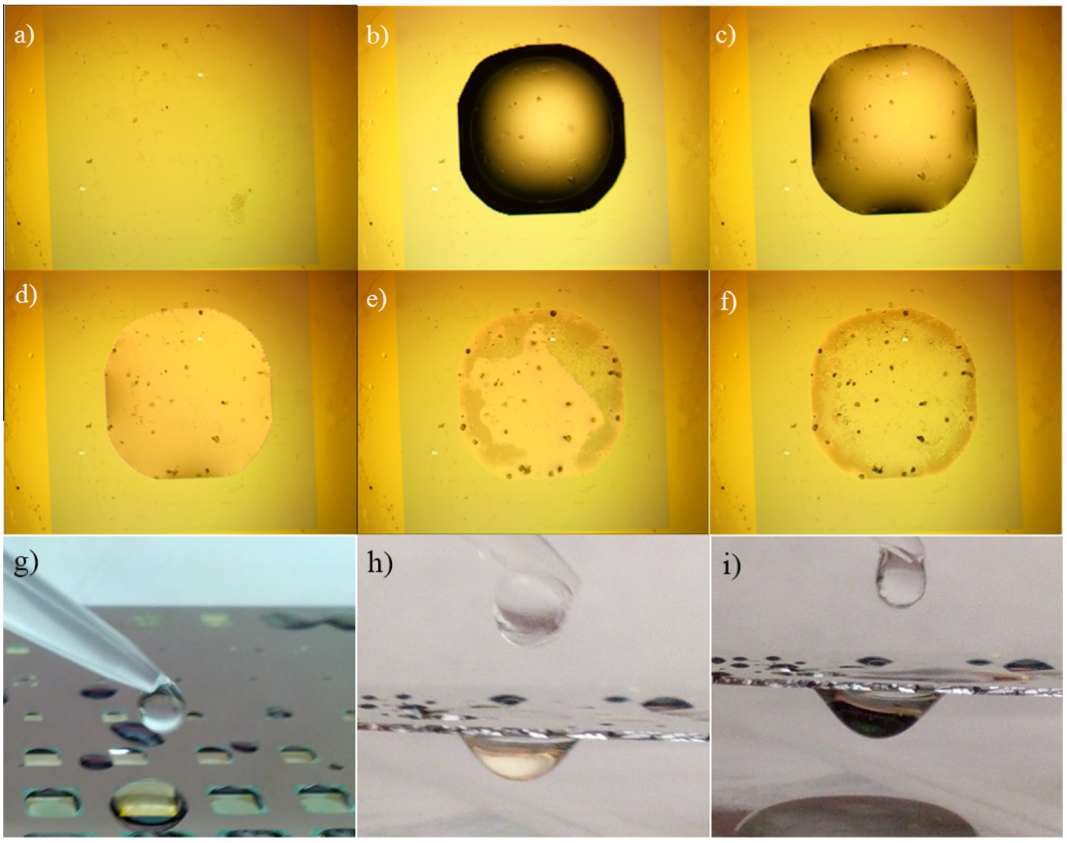

Fig. 6. Demonstration of successful filtration using microfluidic membrane – while water goes through the membrane for further analysis, all the contamination stays on the surface.

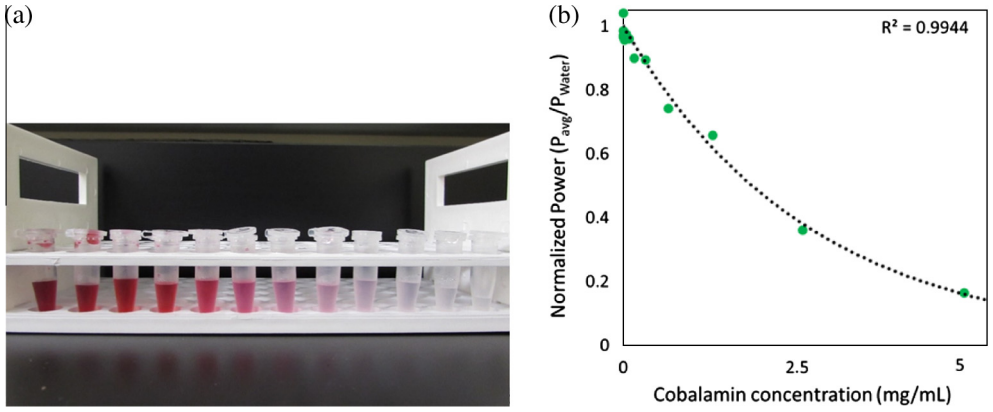

Fig. 7. (a) Samples of different concentrations of cobalamin arranged in order of decreasing concentration. (b) Corresponding experimental results of optical measurements of cobalamin concentration.

Fig. 7a shows the solutions of cobalamin used in this experiment in order of decreasing concentration (left to right). As a results, the experimental points are well fitted by the theoretical curve obtained using Beer–Lambert Law (R^2 = 0.994).

4. Conclusion

In conclusion, we presented a new optofluidic platform for near-patient drug monitoring designed with the purpose of providing additional level of safety for drug administration and decreased human error. This has the potential of reducing preventable deaths due to medical errors. By combining spectroscopic analysis with microfluidic filtration, the system allows rapid and accurate testing for drug concentrations levels. Design, optimization, fabrication and experimental testing of this system for the measurement of cobalamin concentration demonstrated that this approach is promising. Furthermore, it opens up a whole area of optofluidic fiber based drug monitoring where future work includes analysis of multiple drugs and their mixtures and integration with syringes and IV-bags.

Conflict of interest

There is no conflict of interest.

Acknowledgements

We appreciate the help of staff from the University of South Florida Nanotechnology Research and Education Center, and also help of John Winskas and Surya Cheemalapati with device fabrication. E. Archibong was supported by the United States National Science Foundation Florida-Georgia Louis Stokes Alliance for Minority Participation (FGLSAMP) Bridge to the Doctorate grant (HRD #1139850) and the Alfred P. Sloan Minority PhD program.

References

[1] L.T. Kohn, J. Corrigan, M. Donaldson, To err is human: Building a safer health system. Committee on Health Care in America. Institute of Medicine, 1999, National Academy Press, Washington (DC).
[2] P. Anderson, T. Townsend, Medication errors: don't let them happen to you, Am. Nurse Today 5 (3) (2010) 23–27.
[3] M.W. Linder, P.E. Keck, Standards of laboratory practice: antidepressant drug monitoring, Clin. Chem. 44 (5) (1998) 1073–1084.
[4] C. Quiñones-Torrelo et al., Development of predictive retention–activity relationship models of tricyclic antidepressants by micellar liquid chromatography, J. Med. Chem. 42 (16) (1999) 3154–3162.
[5] S. Pankey et al., Quantitative homogeneous enzyme immunoassays for amitriptyline, nortriptyline, imipramine, and desipramine, Clin. Chem. 32 (5) (1986) 768–772.
[6] M.L. Rao et al., Monitoring tricyclic antidepressant concentrations in serum by fluorescence polarization immunoassay compared with gas chromatography and HPLC, Clin. Chem. 40 (6) (1994) 929–933.
[7] F.B. Myers, L.P. Lee, Innovations in optical microfluidic technologies for point-of-care diagnostics, Lab Chip 8 (12) (2008) 2015–2031.
[8] W.F. Crismore, et al., Electrochemical biosensor test strip, 2001, Google Patents.
[9] E.M. Fenton et al., Multiplex lateral-flow test strips fabricated by two-dimensional shaping, ACS Appl. Mater. Interfaces 1 (1) (2009) 124–129.
[10] A.W. Martinez, S.T. Phillips, G.M. Whitesides, Three-dimensional microfluidic devices fabricated in layered paper and tape, Proc. Natl. Acad. Sci. USA 105 (50) (2008) 19606–19611.
[11] H.A. Stone, A.D. Stroock, A. Ajdari, Engineering flows in small devices: microfluidics toward a lab-on-a-chip, Annu. Rev. Fluid Mech. 36 (2004) 381–411.
[12] H. Jiang, X. Weng, D. Li, Microfluidic whole-blood immunoassays, Microfluid. Nanofluid. 10 (5) (2011) 941–964.
[13] R.J. McNichols, G.L. Cote, Optical glucose sensing in biological fluids: an overview, J. Biomed. Opt. 5 (1) (2000) 5–16.
[14] M.R. Robinson et al., Noninvasive glucose monitoring in diabetic patients: a preliminary evaluation, Clin. Chem. 38 (9) (1992) 1618–1622.
[15] A. Pyayt, Electro-optic polymer microring resonators made by photobleaching, in: Integrated Optoelectronic Devices, International Society for Optics and Photonics, 2007.
[16] C.F. Carlborg et al., A packaged optical slot-waveguide ring resonator sensor array for multiplex label-free assays in labs-on-chips, Lab Chip 10 (3) (2010) 281–290.
[17] Y. Sun, X. Fan, Optical ring resonators for biochemical and chemical sensing, Anal. Bioanal. Chem. 399 (1) (2011) 205–211.
[18] A. Pyayt et al., Optical micro-resonator chemical sensor, in: Defense and Security Symposium, International Society for Optics and Photonics, 2007.
[19] M. Scullion, A. Di Falco, T. Krauss, Slotted photonic crystal cavities with integrated microfluidics for biosensing applications, Biosens. Bioelectron. 27 (1) (2011) 101–105.
[20] D. Fattal et al., Guided-mode resonance sensor with extended spatial sensitivity, in: Optics East 2007, International Society for Optics and Photonics, 2007.
[21] J. Stewart, A. Pyayt, Photonic crystal based microscale flow cytometry, Opt. Express 22 (11) (2014) 12853–12860.
[22] S. Shopova et al., Plasmonic enhancement of a whispering-gallery-mode biosensor for single nanoparticle detection, Appl. Phys. Lett. 98 (24) (2011) 243104.
[23] V. Dantham et al., Taking whispering gallery-mode single virus detection and sizing to the limit, Appl. Phys. Lett. 101 (4) (2012) 043704.
[24] S. Holler et al., Label-free single cancer marker protein detection using a nanoplasmonic-photonic hybrid whispering gallery mode biosensor, in: SPIE Sensing Technology + Applications, International Society for Optics and Photonics, 2014.
[25] N. Liu et al., Infrared perfect absorber and its application as plasmonic sensor, Nano Lett. 10 (7) (2010) 2342–2348.
[26] James C. Kraner, Daniel J. McCoy, Michael A. Evans, Linda E. Evans, Brenda J. Sweeney, Fatalities caused by the MDMA-related drug paramethoxyamphetamine (PMA), J. Anal. Toxicol. 25 (7) (2001) 645–648.
[27] Donna. Wielbo, Ian R. Tebbett, The use of microcrystal tests in conjunction with Fourier transform infrared spectroscopy for the rapid identification of street drugs, J. Forensic Sci. 37 (4) (1992) 1134.
[28] Hildebert. Wagner, Plant drug analysis: a thin layer chromatography atlas, Springer, 1996.
[29] Yvan Gaillard, Gilbert Pépin, Screening and identification of drugs in human hair by high-performance liquid chromatography—photodiode-array UV detection and gas chromatography—mass spectrometry after solid-phase extraction a powerful tool in forensic medicine, J. Chromatogr. A762 (1) (1997) 251–267.
[30] Daniel J. Weston, Robert. Bateman, Ian D. Wilson, Tim R. Wood, Colin S. Creaser, Direct analysis of pharmaceutical drug formulations using ion mobility spectrometry/quadrupole-time-of-flight mass spectrometry combined with desorption electrospray ionization, Anal. Chem. 77 (23) (2005) 7572–7580.
[31] Jan K. Maurin, Franciszek Pluciński, Aleksander P. Mazurek, Zbigniew Fijałek, The usefulness of simple X-ray powder diffraction analysis for counterfeit control—The Viagra® example, J. Pharm. Biomed. Anal. 43 (4) (2007) 1514–1518.
[32] S. Coticone, B. Morgan, N. Ludwigsen, Forensic applications of vibrational spectroscopy techniques to identify prescription drugs and mixtures, Int. J. Forensic Sci. 4 (2) (2011).
[33] S. Scafi, C. Pasquini, Identification of counterfeit drugs using near-infrared spectroscopy, Analyst 126 (12) (2001) 2218–2224.
[34] U. Holzgrabe, R. Deubner, C. Schollmayer, B. Waibel, Quantitative NMR spectroscopy – applications in drug analysis, J. Pharm. Biomed. Anal. 38 (5) (2005) 806–812.
[35] Michael D. Hargreaves, Kristian. Page, Tasnim. Munshi, Richard. Tomsett, Gary. Lynch, Howell G.M. Edwards, Analysis of seized drugs using portable Raman spectroscopy in an airport environment—a proof of principle study, J. Raman Spectrosc. 39 (7) (2008) 873–880.
[36] J.T. Motz et al., Optical fiber probe for biomedical Raman spectroscopy, Appl. Opt. 43 (3) (2004) 542–554.
[37] J.G. Fujimoto, Optical coherence tomography for ultrahigh resolution in vivo imaging, Nat. Biotechnol. 21 (11) (2003) 1361–1367.
[38] M. Li et al., Single cell Raman spectroscopy for cell sorting and imaging, Curr. Opin. Biotechnol. 23 (1) (2012) 56–63.
[39] A. Myakov et al., Fiber optic probe for polarized reflectance spectroscopy in vivo: design and performance, J. Biomed. Opt. 7 (3) (2002) 388–397.
[40] S.O. Konorov et al., Hollow-core photonic crystal fiber-optic probes for Raman spectroscopy, Opt. Lett. 31 (12) (2006) 1911–1913.
[41] M.A. Nash et al., Multiplexed enrichment and detection of malarial biomarkers using a stimuli-responsive iron oxide and gold nanoparticle reagent system, ACS Nano 6 (8) (2012) 6776–6785.
[42] Kunda, S.G., Charles; Lynch, Sandra; Siegel, Neal An Ultrasensitive Immunoassay Detection System for Biomarkers Utilizing Raman Scattering Methods. American Laboratory, 2012.
[43] P. Das et al., Designing a thiol specific fluorescent probe for possible use as a reagent for intracellular detection and estimation in blood serum: kinetic analysis to probe the role of intramolecular hydrogen bonding, Org. Biomol. Chem. 11 (38) (2013) 6604–6614.
[44] Surya Cheemalapati et al., Optimization of dry etching parameters for fabrication of polysilicon waveguides with smooth sidewall using capacitively coupled plasma reactor, Appl Optics. 53 (25) (2014) 5745–5749.
[45] H.D. Tong et al., Silicon nitride nanosieve membrane, Nano Lett. 4 (2) (2004) 283–287.
[46] http://www.drugs.com/dosage/cyanocobalamin.html